UNIVERSITY OF HAMBURG
DEPARTMENT OF PHYSICS

Bachelor's Thesis in Physics

Investigation of the influence of crystal quality on Borrmann Spectroscopy

(Untersuchung des Einflusses der Kristallqualität auf Borrmann Spektroskopie)

submitted by

Aram KALAYDZHYAN

1st advisor: Prof. Dr. Edgar WECKERT
2nd advisor: Dr. Martin TOLKIEHN

Hamburg
2012

Erklärung zur Eigenständigkeit

Hiermit bestätige ich, dass die vorliegende Arbeit von mir selbständig verfasst wurde und ich keine anderen als die angegebenen Hilfsmittel – insbesondere keine im Quellenverzeichnis nicht benannten Internet-Quellen – benutzt habe und die Arbeit von mir vorher nicht einem anderen Prüfungsverfahren eingereicht wurde. Die eingereichte schriftliche Fassung entspricht der auf dem elektronischen Speichermedium. Ich bin damit einverstanden, dass die Bachelorarbeit veröffentlicht wird.

Acknowledgements

I would like to thank Prof. Dr. Edgar Weckert for giving me the opportunity to do this project. I gratefully acknowledge the tireless guiding of this work by my supervisor Dr. Martin Tolkiehn. I also thank Torsten Laurus for our numerous discussions of physical and technical issues of this thesis. Finally, I would like to thank my parents, brother and friends from Lomonosov Moscow State University who have supported me in my decision to change the university two years ago.

Abstract

Investigation of the influence of crystal quality on Borrmann Spectroscopy.

The goal of thesis is to apply the dynamical theory of X-ray diffraction for perfect crystals to mosaic crystals, which are composed of slightly misoriented blocks. For this purpose statistical methods were used for the description of crystal defects. This concept was combined with the diffraction theory and implemented in code. This program was used for numerical simulations of diffraction processes in transmission geometry by plane barium titanate crystals. The computed dependencies on defects for Borrmann spectroscopy satisfy the initial expectations for medium orders of crystal defects qualitatively.

Zusammenfassung

Untersuchung des Einflusses der Kristallqualität auf Borrmann Spektroskopie.

Das Ziel dieser Arbeit ist die dynamische Theorie der Röntgenbeugung für perfekte Kristalle auf Mosaikkristalle, die aus leicht fehlohrientierten Blöcken zusammengesetzt sind, anzuwenden. Zu diesem Zweck wurden statistische Methoden zur Beschreibung von Kristalldefekten verwendet und mit der dynamischen Beugungstheorie kombiniert. Darauf basierend wurden numerische Simulationen der Beugungsrozesse in Transmissionsgeometrie für flache Bariumtitanat-Kristalle durchgeführt. Die berechneten Abhängigkeiten von Defekten für Borrmann-Spektroskopie erfüllen qualitativ die Erwartungen für Kristalldefekte mittleren Grades.

Contents

1 Inroduction **1**

2 Theory **2**

2.1 Crystal model 2
2.2 Maxwell's equations 3
2.3 Dispersion Surface 4
2.4 Geometrical properties 7
2.5 Boundary conditions at the entrance surface 7
2.6 Absorption 9
2.7 Boundary conditions at the exit surface 10
2.8 Mosaic crystal 11

3 Barium titanate **13**

3.1 Structure and phase transitions 13
3.2 Mosaic structure 14

4 Simulation **16**

4.1 Formation of the crystal model 16
4.2 Lattice structure factor 17
4.3 Propagation grid 18
4.4 Results 18

5 Conclusion and Outlook **22**

A Source code **23**

Bibliography **35**

Chapter 1

Inroduction

Many crystals of scientific interest lack the high degree of regularity to be ideally perfect, which caused by defects. The geometry of the diffraction effects observed with these crystals in Borrmann spectroscopy is in complete agreement with the dynamical theory for perfect crystals. However, crystal defects provoke quantitative deviations of measured values from theoretical expectations. The aim of this work is to define qualitative variations of Borrmann spectroscopy characteristics with crystal perfection by using of numerical simulations. This thesis is organized as follows. *Chapter 2* explains the main points of the dynamical diffraction theory for perfect crystals and introduces to mosaic models of crystals with defects. *Chapter 3* is devoted to description of the crystal structure of barium titanate, which was selected as a particular case for investigations made in this work. In *Chapter 3* schemes of numerical simulations will be discussed. The results of these computations will be presented in the same chapter.

Chapter 2

Theory

There are basically two different theories for describing X-ray diffraction by crystals. The first one, kinematical theory, was suggested by Darwin in 1914 [1]. He has explained a reflection of X-rays by crystals as their scattering on parallel planes of a crystal. The shortcoming of this model consists in the omitting of multiply scattering effects and interference of the scattered waves. This is the reason why kinematical theory is not suitable for relatively large crystals. A theory, which takes complete account of interference in the infinite crystal, was created by Ewald in 1917 [2] and by von Laue in 1931 [3] and was called as a dynamical theory of X-ray diffraction. The dynamical theory was generalized in the books of Authier [4], Pinsker [5] and Zachariasen [6] and summarized in the article of Batterman and Cole [7]. In terms of this theory it is possible to describe the Borrmann effect [8, 9], a phenomenon of an anomalous increase in the intensity of transmitted through a perfect crystal X-rays satisfying Bragg's law. In the next section I will present the basic principles of dynamical theory for the transmission geometry of diffraction.

2.1 Crystal model

In the dynamical theory the following model of crystal structure is used. We observe a perfect crystal, which is electrically neutral in absence of external field. An incident electromagnetic wave will induce the electron density redistribution. Electrons will oscillate and become dipoles. However we will neglect an influence of X-ray waves to an atomic nucleus. For the description of the electron density in every point of the three-dimensional crystal one should introduce the function $\rho(\mathbf{r})$.

An ideal crystal is defined as an infinite medium with translational symmetry, which consist of identical cells (single or several atoms, molecules etc.). These unit cells are situated with an invariable translation symmetry, which is described by three linearly independent space vectors $\mathbf{a}_i$. Every unit cell is displaced from another one with a distance defined by translation vector:

$$\mathbf{T} := n_1\mathbf{a_1} + n_2\mathbf{a_2} + n_3\mathbf{a_3} \tag{2.1}$$

where n_i are arbitrary integers. The translation symmetry also applies to the electron density function:

$$\rho(\mathbf{r}+\mathbf{T}) = \rho(\mathbf{r}). \tag{2.2}$$

This fact gives us the possibility to express $\rho(\mathbf{r})$ as a Fourier sum over the reciprocal lattice:

$$\rho(\mathbf{r}) = \frac{1}{V}\sum_{\mathbf{H}} F_{\mathbf{H}}\, e^{-2\pi i \mathbf{H}\cdot\mathbf{r}} \tag{2.3}$$

where $V = |\mathbf{a_1}\cdot\mathbf{a_2}\times\mathbf{a_3}|$ is the volume of the unit cell and **H** is a reciprocal lattice vector, which is defined as

$$\mathbf{H} := h\mathbf{b_1} + k\mathbf{b_2} + l\mathbf{b_3} \tag{2.4}$$

where $\mathbf{b}_i = \dfrac{1}{V}\sum_{j,k}\epsilon_{ijk}(\mathbf{a}_j\times\mathbf{a}_k)$ are the reciprocal lattice vectors and *h, k, l* are the Miller indices, ϵ_{ijk} is the Levi-Civita symbol. The Fourier coefficients in (2.3) are the structure factors, given by

$$F_{\mathbf{H}} = \int\limits_V \rho(\mathbf{r}) e^{2\pi i \mathbf{H}\cdot\mathbf{r}} dv, \tag{2.5}$$

Suppose the atoms are not vibrating thermally; then $F_{\mathbf{H}}$ can be written as

$$F_{\mathbf{H}} = \sum_n f_n e^{2\pi i \mathbf{H}\cdot\mathbf{r}_n}, \tag{2.6}$$

where the sum is over every n-th atom in the unit cell with the atomic scattering factor f_n. Geometry of the unit cell and structure factors define an influence of crystal medium on the incident electromagnetic wave, which is described in the next section.

2.2 Maxwell's equations

The X-ray wave in a crystal should satisfy macroscopic Maxwell's equations

$$\begin{aligned} curl\ \mathbf{E} &= -\frac{\partial \mathbf{B}}{\partial t} \\ curl\ \mathbf{H} &= \frac{\partial \mathbf{D}}{\partial t} + \mathbf{j}_f \\ div\ \mathbf{D} &= \rho_f \\ div\ \mathbf{B} &= 0, \end{aligned} \tag{2.7}$$

where **E** is the electric field, **B** is the magnetic induction, **D** is the electric displacement and **H** is the magnetic field; ρ_f is free charge density, which is in our case equal $\rho(\mathbf{r})$ defined in the previous section, $\mathbf{j}_f$ is free current density caused by moving of free charges. The electron density redistribution causes a polarization **P** and is connected with **E** and **D** by the material relation:

$$\mathbf{D}(\mathbf{r}) = \epsilon\mathbf{E}(\mathbf{r}) = \epsilon_0\mathbf{E}(\mathbf{r}) + \mathbf{P}(\mathbf{r}) = \epsilon_0(1+\chi(\mathbf{r}))\mathbf{E}(\mathbf{r}) \tag{2.8}$$

where χ is the polarizability function, ϵ_0 and ϵ are the dielectric constants of the vacuum and the medium, respectively. Assuming that the incident wave is a plane wave and that the frequency of this wave is always far from the resonance frequencies of electrons, it is possible (see [4]) to deduce that $\chi(\mathbf{r})$ is proportional to the electron density function

$$\chi(\mathbf{r}) = -\frac{r_e \lambda^2}{\pi} \rho(\mathbf{r}), \tag{2.9}$$

where $r_e \approx 2.82 \times 10^{-15}\ m$ is the Thomson scattering length. It means that $\chi(\mathbf{r})$ is periodic too and can be expressed as Fourier sum with coefficients

$$\chi_h = -\frac{r_e \lambda^2}{\pi} F_H = -\Gamma F_H, \ \ \Gamma := \frac{r_e \lambda^2}{\pi}, \tag{2.10}$$

where λ is the wavelength. In addition, we suppose that

$$div\ \mathbf{E} = 0 \tag{2.11}$$

because the crystal is electrically neutral.

Combining (2.8), (2.11) and the first two Maxwell's equations (2.7), one can obtain the propagation equation for the electric field of the electromagnetic wave

$$\begin{aligned} \Delta \mathbf{D} + \text{curl curl}\ \chi(\mathbf{r})\mathbf{D} + 4\pi^2 k^2 \mathbf{D} = 0, \\ \text{curl curl}\ \mathbf{E} - 4\pi^2 k^2 (1 + \chi(\mathbf{r}))\mathbf{E} = 0, \end{aligned} \tag{2.12}$$

where $k = \frac{1}{\lambda}$.

2.3 Dispersion Surface

The solution of (2.12) for each X-ray wave with wave vector $\mathbf{K_0}$ is a Bloch-Ewald wave:

$$\mathbf{D} = \sum_{\mathbf{H}} \mathbf{D_H} e^{-2\pi i (\mathbf{K_0} + \mathbf{H}) \cdot \mathbf{r}} \tag{2.13}$$

Now we shall give the following definition for simplifying of following equations:

$$\mathbf{K_H} := \mathbf{K_0} + \mathbf{H} \tag{2.14}$$

From (2.8), (2.10) and (2.12) after inserting of the ansatz (2.13) it follows that

$$[k^2(1 - \Gamma F_0) - (\mathbf{K_H} \cdot \mathbf{K_H})]\mathbf{E_H} - k^2 \Gamma \sum_{\mathbf{P} \neq \mathbf{H}} F_{H-P} \mathbf{E_P} + (\mathbf{K_H} \cdot \mathbf{E_H})\mathbf{K_H} = 0 \tag{2.15}$$

This is a general vector equation with complex components, which is describing the electric field inside the crystal. This system can be solved only after introducing additional conditions.

Now we introduce a concept to pass from general set of equations (2.15) to particular form. Firstly, we will analyze only one active reflection. In other words, we consider that all field amplitudes inside the crystal could be disregarded except only $\mathbf{E_0}$ and $\mathbf{E_H}$. Additionally, we will make a restriction, which is that we discuss the components of $\mathbf{E_0}$ and $\mathbf{E_H}$ normal to the plane of incidence (the σ polarization). The calculus for parallel polarization state (π polarization) is analog to the case of the σ polarization and will be omitted. Now it is possible to convert equation set (2.15) to an particular form according to the stated conditions:

$$\begin{aligned} [k^2(1-\Gamma F_0) - (\mathbf{K_0}\cdot\mathbf{K_0})]E_0 - k^2\Gamma F_{\overline{H}} E_H = 0 \\ -k^2\Gamma F_H E_0 + [k^2(1-\Gamma F_0) - (\mathbf{K_H}\cdot\mathbf{K_H})]E_H = 0 \end{aligned} \tag{2.16}$$

For non-trivial solution of this system of linear equations the determinant of (2.16) must be equal to zero:

$$\begin{vmatrix} k^2(1-\Gamma F_0) - \mathbf{K_0}\cdot\mathbf{K_0} & -k^2\Gamma F_{\overline{H}} \\ -k^2\Gamma F_H & k^2(1-\Gamma F_0) - \mathbf{K_H}\cdot\mathbf{K_H} \end{vmatrix} = 0 \tag{2.17}$$

Suppose $\sqrt{\mathbf{K_0}\cdot\mathbf{K_0}} + k\sqrt{1-\Gamma F_0} \approx 2k$ we denote the diagonal elements of the determinant (2.17)

$$\begin{aligned} 2k\xi_0 := \mathbf{K_0}\cdot\mathbf{K_0} - k^2(1-\Gamma F_0) \approx 2k[\sqrt{\mathbf{K_0}\cdot\mathbf{K_0}} - k(1-\tfrac{1}{2}\Gamma F_0)] \\ 2k\xi_H := \mathbf{K_H}\cdot\mathbf{K_H} - k^2(1-\Gamma F_0) \approx 2k[\sqrt{\mathbf{K_H}\cdot\mathbf{K_H}} - k(1-\tfrac{1}{2}\Gamma F_0)] \end{aligned} \tag{2.18}$$

and reduce it to the equation of the dispersion surface in reciprocal space

$$\xi_0\xi_H = \frac{1}{4}k^2\Gamma^2 F_H F_{\overline{H}}, \tag{2.19}$$

which describes two three-dimensional surfaces of revolution. It is useful to show graphically a two-dimensional slice of the dispersion surface in the reciprocal space. In a general case, ξ_0 and ξ_H are complex and only their real parts will be plotted. The point O in Fig.2.1 (left) is the origin. The point H corresponds to the reciprocal lattice point (hkl) and, by definition, $\mathbf{H} = \mathbf{OH}$. The point L_a is situated in the equal distance k from both O and H and is called the Laue point. An incident wave with wave vector $\mathbf{L_aO}$ and a reflected wave with wave vector $\mathbf{L_aH}$ are describing the Bragg reflection. According to the geometrical theory of diffraction, an angle between these two vectors is equal $2\theta_B$, where θ_B is the angle between the incident ray and the lattice planes in such a case when Bragg peak is produced. Bragg's law binds θ_B with the wavelength of the incident beam λ and the spacing d_{hkl} between (hkl) planes of the crystal lattice:

$$\sin\theta_B = \frac{\lambda}{2\,d_{hkl}} \tag{2.20}$$

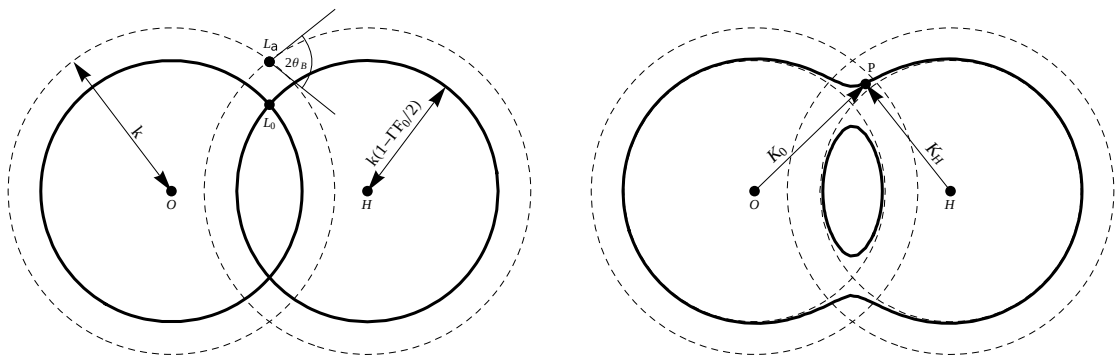

Figure 2.1: Diffraction scheme in reciprocal space. O: origin; P: reciprocal lattice point (hkl). *(left)* L_a: Laue point; $\mathbf{OL_a}$ and $\mathbf{HL_a}$, respectively, incident and reflected waves satisfy Bragg's condition in the kinematical theory; *(right)* P: a point on the dispersion surface by the dynamical theory (solid curve); $\mathbf{OP}$ and $\mathbf{HP}$, respectively, incident and reflected waves.

Solid circles in Fig.2.1 (left) have centers in O and H and the same radius $k(1 - \frac{1}{2}\Gamma F_0)$. The point of their intersection L_0 is called Lorentz point. Suppose $\mathbf{K_0} = \mathbf{OP}$ and $\mathbf{K_H} = \mathbf{HP}$; then the distances between the point P and intersections of $\mathbf{K_0}$ and $\mathbf{K_H}$ with the circles are defined by ξ_0 and ξ_H, respectively. In general, 2.19 describes two hyperbolic sheets in the region of L_0, which are asymptotically approaching to the circles (Fig. 2.1, right). The sheet which lies in the same side of asymptotes as the Laue point is called α branch. Real parts of ξ_0 and ξ_H are positive at this branch. For the other sheet, called β branch, real parts of ξ_0 and ξ_H are negative. Let us remark that Fig. 2.1 has only qualitative nature, because the distance between the hyperbolic sheets is unnoticeable on a scale of $\mathbf{OH}$. An example of real dispersion surface is presented in Fig. 2.2.

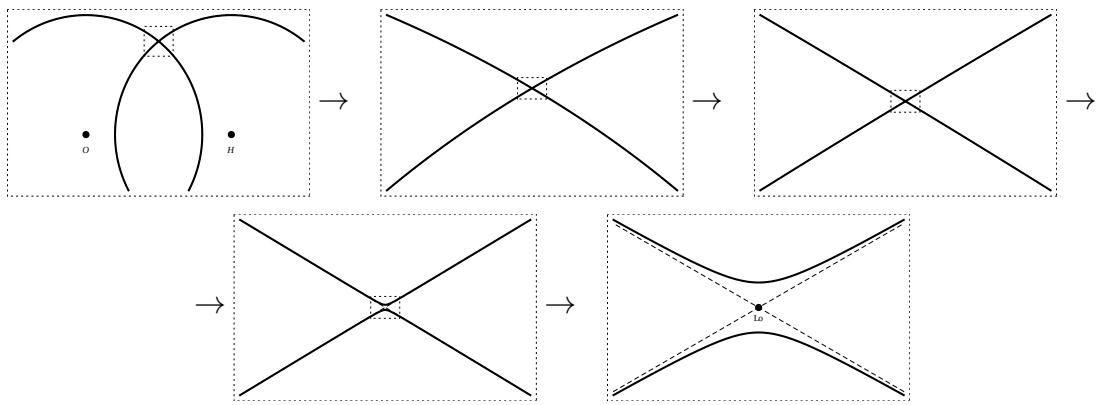

Figure 2.2: The dispersion surface for $BaTiO_3$-crystal (200 reflection, 4.9 keV) with different scalings. The zone selected by the dashed rectangle in the first figure is shown in the next figure with 10x scaling. Only after the third repeating of this operation (10000x scaling) the branches of the dispersion surface are plainly distinguishable.

2.4 Geometrical properties

Now we note that in the current work we are analyzing the diffraction effect in a crystal with parallel surfaces. The incident wave can be arbitrarily oriented to the selected diffraction plane of the crystal. Nevertheless we are observing only the case of the σ polarization of the incident light. An angle between them will be expressed in terms of $\Delta\theta$, which is the deviation from Bragg's angle of the incident wave (see Fig. 2.3, left). The diffraction plane can be also arbitrarily oriented to the crystal surface. An angle between these two planes will be designated as ω (see Fig. 2.3, right). Suppose the reflected wave is directed towards the inside of crystal. Such a diffraction geometry is called transmission, or Laue, geometry. Let $\gamma_0 := \mathbf{n} \cdot \mathbf{s_0}$ and $\gamma_H := \mathbf{n} \cdot \mathbf{s_H}$, where $\mathbf{s_0}$ and $\mathbf{s_H}$ are unit vectors in the incident and diffraction beam directions and $\mathbf{n}$ is the surface normal; then they could be expressed in terms of $\Delta\theta$, θ_B and ω:

$$\begin{aligned} \gamma_0 &= \cos(\Delta\theta + \omega + \theta_B) \\ \gamma_H &= \cos(\Delta\theta + \omega - \theta_B) \end{aligned} \tag{2.21}$$

Their relation is called asymmetry ratio and is designated in literature either γ (e.g. in [4]) or b (e.g. in [7]):

$$b = \gamma^{-1} := \frac{\gamma_0}{\gamma_H} = \frac{\cos(\Delta\theta + \omega + \theta_B)}{\cos(\Delta\theta + \omega - \theta_B)} \tag{2.22}$$

The factor b^{-1} appears for the ratios of the cross-sections for the incident and the reflected waves (see Fig. 2.4). Additionally the asymmetry ratio will be often used below for reduction of computations.

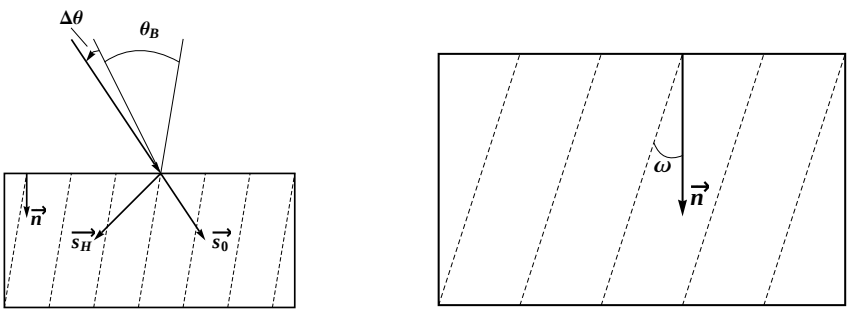

Figure 2.3: Diffraction in transmission (Laue) geometry. $\mathbf{n}$: the normal to the crystal surface; $\mathbf{s_0}$ and $\mathbf{s_H}$: unit vectors in the incident and diffraction beam directions; $\Delta\theta$: deviation from Bragg's angle of the incident wave; ω: angle between $\mathbf{n}$ and lattice planes (dashed)

2.5 Boundary conditions at the entrance surface

Electromagnetic waves are transmitted and reflected at a boundary between vacuum and crystal media. We assume that the incident wave is a plane wave, which completely penetrates to the crystal. This implies the following boundary conditions for field amplitudes (see the full

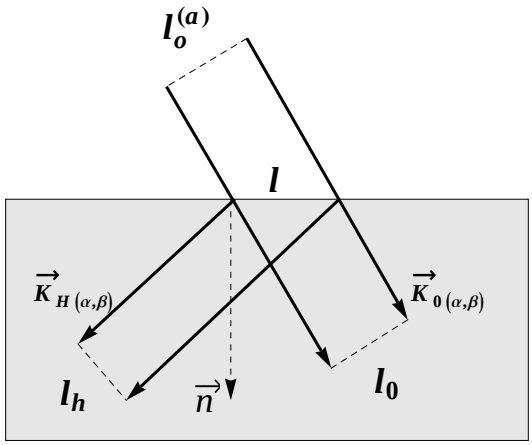

Figure 2.4: The cross-sections $l_0^{(a)}$, l_0 and l_h of the incident, refracted and reflected waves, respectively. Suppose l is the width of the beam trace on the crystal surface; then it is not hard to prove that $l_0 = l\gamma_0 = l_0^{(a)}$ and $l_h = l\gamma_h = b^{-1}l_0^{(a)}$.

proving at [4]):

$$\begin{aligned} \mathbf{E}_0^{(a)} &= \mathbf{E}_{0\alpha} + \mathbf{E}_{0\beta} \\ 0 &= \mathbf{E}_{H\alpha} + \mathbf{E}_{H\beta}, \end{aligned} \tag{2.23}$$

where $\mathbf{E}_0^{(a)}$ is the amplitude of the incident wave, $\mathbf{E}_{0\alpha}$ and $\mathbf{E}_{0\beta}$ for the refracted waves and $\mathbf{E}_{H\alpha}$ and $\mathbf{E}_{H\beta}$ for reflected waves by α and β branches, respectively. If one combine this with 2.16, one gets

$$\begin{aligned} E_{0(\alpha,\beta)} &= \frac{\sqrt{1+\eta^2} \mp \eta}{2\sqrt{1+\eta^2}} E_0^{(a)}, \\ E_{H(\alpha,\beta)} &= \pm \frac{\sqrt{F_H F_{\overline{H}}}}{F_{\overline{H}}} \frac{\sqrt{b}}{2\sqrt{1+\eta^2}} E_0^{(a)}, \end{aligned} \tag{2.24}$$

where η, called asymmetry ratio, is defined as

$$\eta := \frac{b\Delta\theta \sin 2\theta + \frac{1}{2}\Gamma F_0(1-b)}{\Gamma\sqrt{|b|}\sqrt{F_H F_{\overline{H}}}}. \tag{2.25}$$

Application of the boundary conditions for wave vectors makes the following term (see the proving at [7]): the components of the wave vectors $\mathbf{K}_{0\alpha}$ and $\mathbf{K}_{0\beta}$ along the crystal surface must equal the surface component of the incident wave vector $\mathbf{K}_0$. This term yields that

$$\begin{aligned} \xi_{0(\alpha,\beta)} &= \tfrac{1}{2}k\Gamma\sqrt{|b|}\sqrt{F_H F_{\overline{H}}}\,[\eta \pm \sqrt{\eta^2 + sgn(b)}], \\ \xi_{H(\alpha,\beta)} &= \tfrac{1}{2}k\Gamma\sqrt{\tfrac{1}{|b|}}\sqrt{F_H F_{\overline{H}}}\,[\eta \pm \sqrt{\eta^2 + sgn(b)}]^{-1}. \end{aligned} \tag{2.26}$$

Thereby, we can have the possibility to write both the amplitudes and the wave vectors of the wavefields inside the crystal in the explicit form.

2.6 Absorption

Let us now analyze behaviour of wavefield intensities inside the crystal. Using (2.18), (2.24) and (2.26) we get the wavefield intensities:

$$\begin{aligned}
\frac{I_{0(\alpha,\beta)}}{I_0^{(a)}} &= \left|\frac{E_{0(\alpha,\beta)}}{E_0^{(a)}} e^{-2\pi i \mathbf{K}_{\mathbf{0}(\alpha,\beta)}\cdot\mathbf{r}}\right|^2 = \left|\frac{E_{0(\alpha,\beta)}}{E_0^{(a)}}\right|^2 e^{-4\pi \mathrm{Im}[k(1-\frac{1}{2}\Gamma F_0)+\chi_{0(\alpha,\beta)}]t/\gamma_0} = \\
&= \left|\frac{\sqrt{1+\eta^2}\mp\eta}{2\sqrt{1+\eta^2}}\right|^2 e^{-\mu^{\mathrm{eff}}_{(\alpha,\beta)}t/\gamma_0}, \qquad (2.27)\\
\frac{I_{H(\alpha,\beta)}}{I_0^{(a)}} &= b^{-1}\left|\frac{E_{H(\alpha,\beta)}}{E_0^{(a)}} e^{-2\pi i \mathbf{K}_{\mathbf{H}(\alpha,\beta)}\cdot\mathbf{r}}\right|^2 = \left|\frac{\sqrt{F_H F_{\overline{H}}}}{F_{\overline{H}}}\frac{1}{2\sqrt{1+\eta^2}}\right|^2 e^{-\mu^{\mathrm{eff}}_{(\alpha,\beta)}t/\gamma_0},
\end{aligned}$$

where t is the depth of the observation point along the $\mathbf{n}$ and effective absorption coefficient $\mu^{\mathrm{eff}}_{(\alpha,\beta)}$ is defined as

$$\mu^{eff}_{(\alpha,\beta)} := \mu_0 - 4\pi \mathrm{Im}[\xi_{0(\alpha,\beta)}], \;\; \mu_0 := 2\pi k \Gamma \mathrm{Im}[F_0]. \qquad (2.28)$$

Let us remark the different behaviours of effective absorption coefficients for α and β branches in the region of an reflexion. In the general case, absorption of the α wavefields in such region decreases (see Fig. 2.5), and, vice versa, increases for the β wavefields. In regions which are far from diffraction reflexions the effective absorption coefficients are asymptotically approaching to μ_0, the mean of absorption coefficients by crystal volume. In a proper combination of the crystal structure and reflexion, absorption of the α wavefields totally disappears (e.g. in the case shown in the Fig. 2.5). This fact theoretically explains existence of the Borrmann

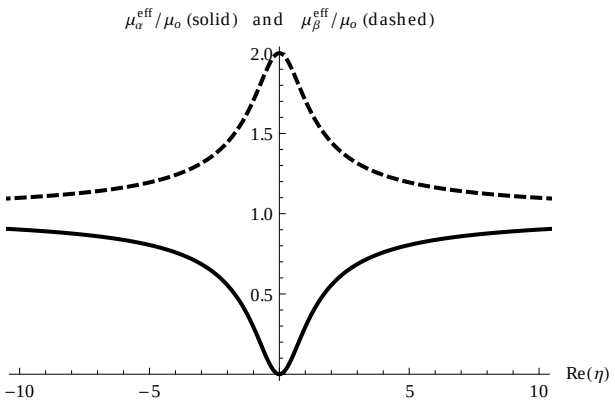

Figure 2.5: Variations of the effective absorption coefficients for α (solid) and β (dashed) branches with the deviation parameter [$BaTiO_3$-crystal, 200 reflection, 4.9 keV, $\omega = 0$]

effect: the α wavefields will reach an exit surface of the crystal without absorption if the incident wave satisfies Bragg's law. We can see in Fig. 2.6 how the effective absorption coefficients influences to the variations of the wavefield intensities with the deviation parameter. There is firstly shown the non-absorbing case ($\mu_0 t = 0$), where I_0 wavefields are symmetric and I_H wavefields perfectly coincide. By increasing of the absorption ($\mu_0 t = 0.5$ and $\mu_0 t = 1$) the more active weakening of β wavefields in the region of $Re(\eta) = 0$ is present.

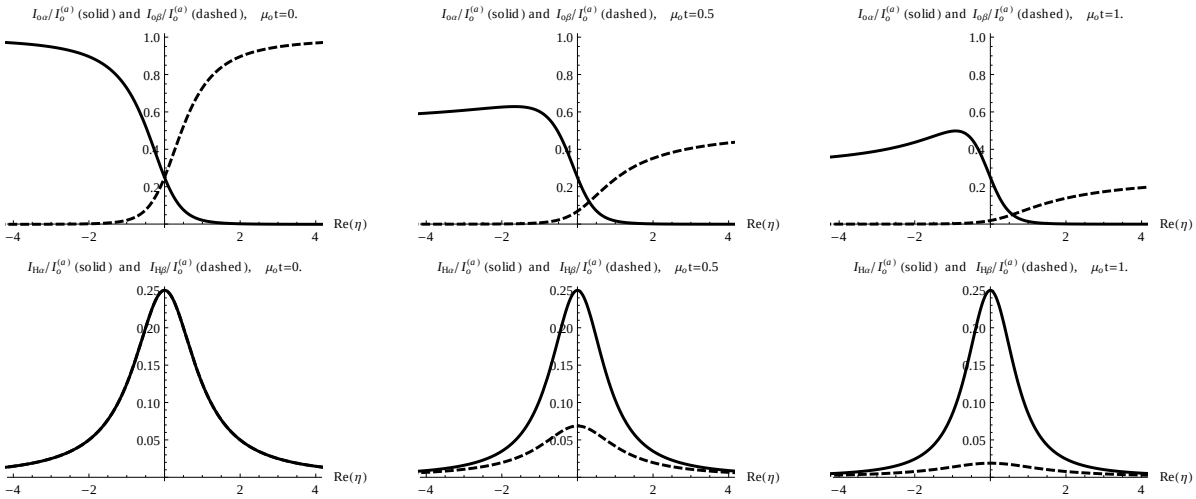

Figure 2.6: Variations of the wavefield intensities with the deviation parameter for the different absorption [$BaTiO_3$-crystal, 200 reflection, 4.9 keV, $\omega = 0$]

2.7 Boundary conditions at the exit surface

For complete diffraction analysis in a single crystal we should discuss how the wavefields are passing through the exit surface to vacuum. Owing to the fact that the input and output surfaces are parallel to each other it is possible to represent an outgoing wavefield as two plane waves with amplitudes $E_0^{(d)}$ and $E_H^{(d)}$. These two waves are results of interference of the wavefields in the the incident and diffraction beam directions, respectively. Boundary conditions at the exit surface are analog to conditions at the entrance surface. Applying the boundary conditions to the amplitudes and the wave vectors of the outgoing wavefields and expressing $E_0^{(d)}$ and $E_0^{(d)}$ in terms of $E_{0(\alpha,\beta)}$ and $E_{H(\alpha,\beta)}$ (see [4]), we get

$$\begin{aligned} E_0^{(d)} &= E_{0\alpha}\, e^{-2\pi i(\xi_{0\alpha}-\frac{1}{2}k\Gamma F_0)t/\gamma_0} + E_{0\beta}\, e^{-2\pi i(\xi_{0\beta}-\frac{1}{2}k\Gamma F_0)t/\gamma_0}, \\ E_H^{(d)} &= E_{H\alpha}\, e^{-2\pi i(\xi_{0\alpha}-\frac{1}{2}k\Gamma F_0)t/\gamma_0} + E_{H\beta}\, e^{-2\pi i(\xi_{0\beta}-\frac{1}{2}k\Gamma F_0)t/\gamma_0}, \end{aligned} \tag{2.29}$$

where t is the crystal thickness. An example of the variations of the wave intensities with the deviation parameter is presented in Fig. 2.7 (left). An important specificity of the outgoing intensities is their antiphased oscillation with the crystal thickness (see Fig. 2.7, right). Such a

phenomenon has been called the Pendellösung by Ewald because of the resemblance with the energy transfer between two pendulums. The period of these oscillations Λ is

$$\Lambda := \frac{1}{\sqrt{1+\mathrm{Re}[\eta]^2}}\Lambda_L, \quad \Lambda_L := \frac{\sqrt{|b|}\cos\theta_B}{k\Gamma\sqrt{F_H F_{\overline{H}}}}. \tag{2.30}$$

where Λ_L is the maximum value of Λ.

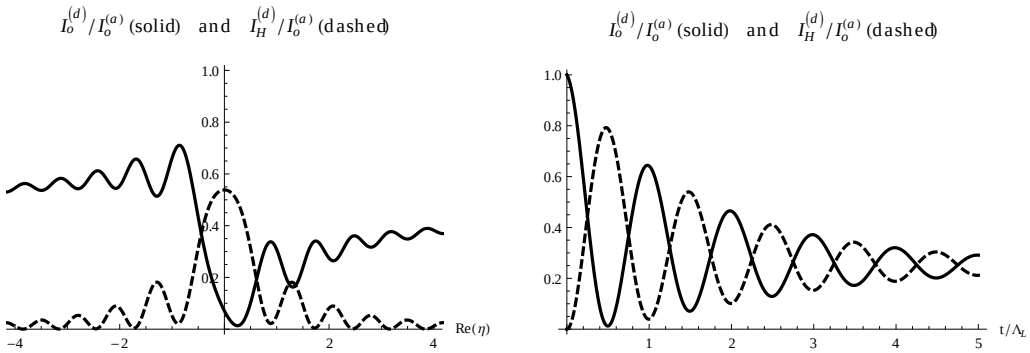

Figure 2.7: Variations of the wave intensities with the deviation parameter for t/Λ_L=1.5 (left) and the Pendellösung for $\eta = 0$ (right) [$BaTiO_3$-crystal, 200 reflection, 4.9 keV, $\omega = 0$]

2.8 Mosaic crystal

The theory of X-ray diffraction for ideal crystals in Laue geometry was discussed in the preceding parts of this chapter. However we should extend the theory to the real, not perfectly ordered crystals. A real crystal is comprised by slightly misoriented blocks, or domains, which can be considered as perfect crystals (see Fig 2.8). Such a crystal is called mosaic crystal (this term was proposed by P. P. Ewald [10]) and there are different possible models for describing of its mosaicity, which will be described in this section.

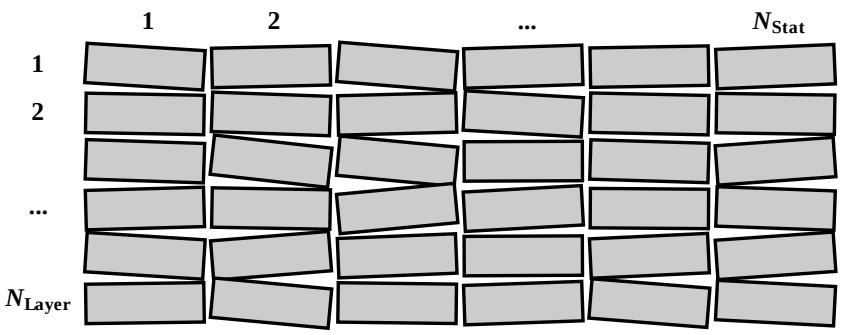

Figure 2.8: The qualitative illustration of the mosaicity phenomenon of the real crystals: domains (gray rectangles), which are the ideal crystals, are slightly misoriented with respect to one another.

The simplest model can be created if we suppose that surfaces of all domains of the crystal are parallel to each other (see Fig. 2.9, *left*). Then the crystal is defined by the set of domain

thickness t_i and lattice orientation ω_i. This model can be slightly modified supposing that all domains have parallel surfaces, but they are slightly misoriented relative to each other by the set of angles α_i (see Fig. 2.9, *center*). We consider, that there is vacuum in the space between the domains. This consideration does not strongly correlate with the real construction of a mosaic crystal. The most correct possibility to describe the real crystal is to suppose that the surfaces are not parallel even in each domain (see Fig. 2.9, *right*). This improved model doesn't required an additional expansion of the parameters describing a mosaic crystal. However, the difference is sensible by a numerical simulation of the wave diffraction by such a crystal.

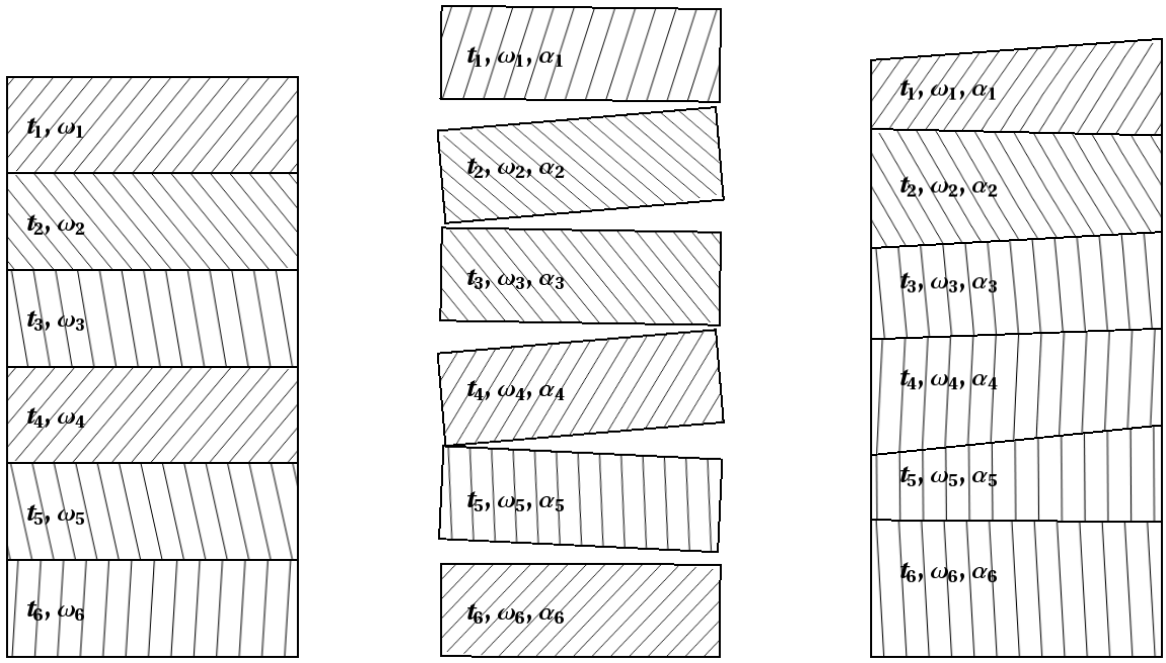

Figure 2.9: Possible simplified models of the mosaic crystals. *(Left)*: all surfaces of all domains are parallel; *(center)*: the domains have parallel surfaces, but are not parallel to each other; *(right)*: all domain surfaces are oriented arbitrarily.

In the first and second cases the number of beams propagating through the crystal is doubled after each domain layer. This fact leads to the total number of simulated diffractions equals $(2^{N_{\text{layers}}+1} - 1)$, where N_{layers} is the number of domain layers. For the case of arbitrary oriented surfaces the number of the beams is quadrupled after the each layer. Therefore, the the total number of simulation grows to $\frac{1}{3}(4^{N_{\text{layers}}+1} - 1)$. In this work we will use the model, where all domain surfaces are parallel to each other, because this model requires the lowest amount of numerical calculations used for the simulation of the diffraction by a mosaic crystal.

Chapter 3

Barium titanate

In this chapter will be introduced the main properties and peculiarities of the barium titanate, the crystal, used in the current work for the numerical modeling and the experimental observing of Borrmann effect. This crystal is a well known [11, 12, 13, 14] mosaic crystal with perovskite-like structure and is in possession of such a mosaicity, that can be increased by the phase transitioning of the crystal.

3.1 Structure and phase transitions

The barium titanate crystals with the chemical formula $\mathrm{BaTiO_3}$ have, as stated above, a perovskite structure, i.e. with the same type of crystal structure as the $\mathrm{CaTiO_3}$ perovskite mineral. The ideal perovskite ABO_3 structure is a cubic network of corner-linked large cations A, with oxygen in the edge centers and the smaller cation B in the center of the unit cell. The unit cell of $\mathrm{BaTiO_3}$ cubic structure is shown below in Fig. 3.1.

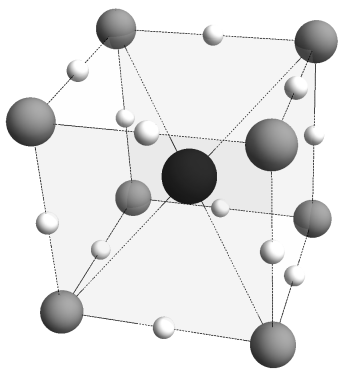

Figure 3.1: Ideal perovskite-like structure of $\mathrm{BaTiO_3}$: The gray spheres are Ti^{4+} cations, black is the Ba^{2+} cation and the white are oxide centers.

However, let us remark that the barium titanate crystals have an ideal cubic structure [11] only by temperatures above the Curie point ($> 120°$C). By the temperature below the Curie

point the cubic $BaTiO_3$ transforms into a tetragonal crystal. The crystal keeps this lattice geometry also for the room temperatures. Cooling through about 5°C causes the tetragonal phase of barium titanate to transform to a orthorhombic phase and to trigonal below -70°C (see Fig. 3.2, *left*).

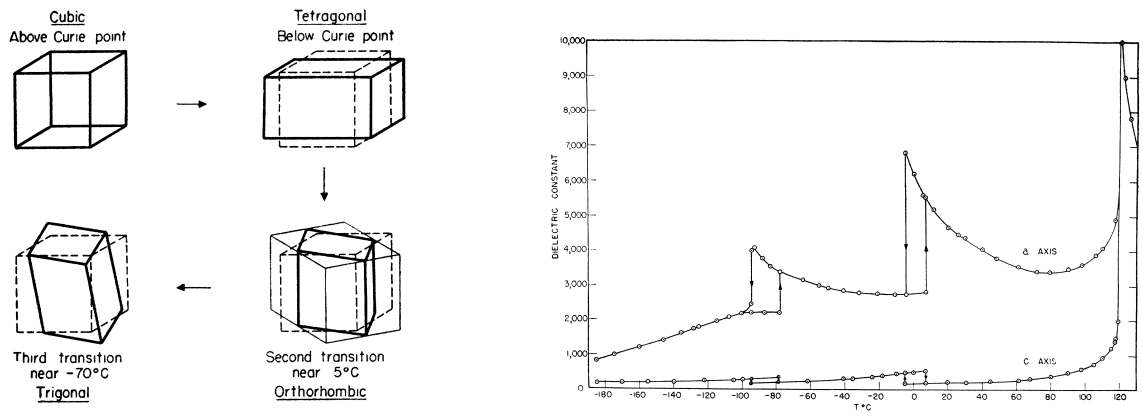

Figure 3.2: (*left*) Deformation of the $BaTiO_3$ unit sell by phase transitions. (*right*) Variations of the dielectric constant parallel to a- and c-axes with the temperature of the barium titanate crystal [11].

The aforementioned phase transitions of $BaTiO_3$ crystal were investigated in detail in several works, for example, by F. W. Forsbergh [12] and A. von Hippel [11]. In the second work the behaviour of the lattice by the transitions was indicated by measurements of the dielectric constant parallel to the different axes of the crystal. The result of this measurements is presented in Fig. 3.2 (*right*). The phase transitions are characterized by sudden changes of the dielectric constant. Let us stress the temperature hysteresis accompany the phase transitions below the Curie point. This phenomenon causes by the complex domain structure of the crystal and reorientation of this domains during the phase transitions.

3.2 Mosaic structure

In number of works, for example, by H. F. Kay [13] and R. G. Rhodes [14], has been argued by means of X-rays, that the originally single crystal of $BaTiO_3$ was breaking down into a multi-domain, mosaic structure by every phase transition. Moreover, this effect appears for both rising and falling temperature, but with the phenomenon of the temperature hysteresis by the low-temperature phase transitions. However, the structure of every domain in the crystal is not changing even after many complete cycles of temperature changing and phase transitions. This feature of the barium titanate crystals can be very helpful for investigations of the effects, that depends on the mosaicity degree of the crystal. Let us now introduce the concept of the experiment, which supposedly give the possibility to lead such investigations by the use of only one sample and changing its mosaicity without interruption of an experiment. As a rule, the $BaTiO_3$ samples are produced nearly as single-domain crystals with the tetragonal internal symmetry at room temperature. It means, that the mosaicity phenomenon for this crystal is

almost absent. Then one should cool down the sample above the temperature of a phase transition and, after that, restore the former temperature. As a result, the single domain of the crystal would be broken into slightly misoriented domains, i.e. the mosaicity of the crystal would be increase, but the internal symmetry of each domain would be still tetragonal. This cycle can be repeated several times with the stepwise augmentation of domain misorientation.

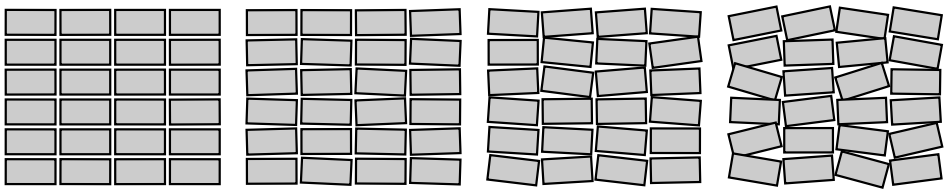

Figure 3.3: The qualitative illustration of the mosaicity increasing (*from left to right*) of the $BaTiO_3$ crystal after the full temperature cycles via a phase transition.

The above-described increasing of the mosaicity influences on X-ray spectroscopy of the crystal, including the Borrmann effect. This complex effect can be numerically simulated and is described in the next chapter.

Chapter 4

Simulation

Suppose a crystal has the mosaic structure; then one should combine the dynamical theory (see Chapter 2) with the probability theory to prognosticate the diffraction process by such a crystal. This complication of the diffraction theory for the mosaic crystals is provoked by the fact, that the structure of the crystal is described statistically. In this case it is too complicated to analyze the diffraction effect analytically. The aim of this chapter is to show how to numerically simulate the diffraction by the mosaic crystal on computer. All simulations were made in *Wolfram Mathematica 8* computation system on computers of DESY (Hamburg) research center. The source codes can be found in the Appendix A. The result of this simulation for the $\mathrm{BaTiO_3}$ mosaic crystals will be presented and discussed in the end of this chapter.

4.1 Formation of the crystal model

For simulation of the mosaic structure we will use the model of the mosaic crystal, which consists of blocks of perfect crystals (domains) with slightly misoriented lattice planes. Let us assume that all surfaces of the domains are parallel to each other (see Fig. 2.9, *left*). We claim that each incident X-ray wave propagate via N_{Layer} layers of the domains with the thickness t_i and the lattice misorientation ω_i (see Fig. 2.3, *right*). Let us note that number of the domains by every layer, that are inside the beam cross-section, carries no physical, but a statistical meaning and will be called N_{Stat}. Suppose the distribution of t_i and ω_i is normal, then we can describe this distribution with parameters of the thickness mean t_μ, its standard deviation t_σ and the standard deviation of the lattice misorientation ω_σ (the mean of ω is equal zero in this work). Therefore, the mosaicity of the crystal model is regulated by parameter ω_σ: the larger it is the more considerable is the mosaicity (see Fig. 4.1). We will set the the standard deviation of ω_i in scales of several thousandths of degree.

The generated distributions of t_i and ω_i fit sufficiently to the ideal normal distribution by large total number of crystal domains $N_{\mathrm{Layer}} \cdot N_{\mathrm{Stat}}$ (see Fig. 4.2). onsequently, for good statistics we should set the N_{Stat} parameter not smaller than couple hundreds.

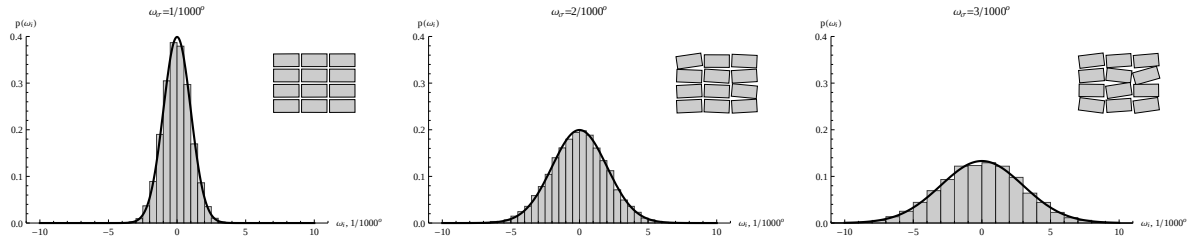

Figure 4.1: Histograms of the generated lattice misorientation ω_i of the crystal domains for different normal distribution ω_σ. Solid line: ideal normal probability distribution. In the corners: respective qualitative illustration of the mosaicity evidence.

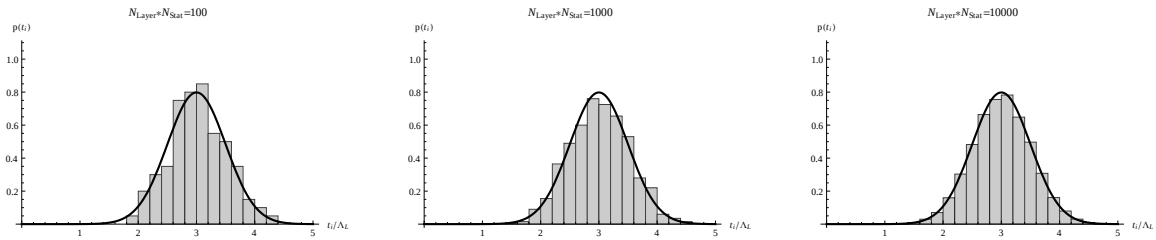

Figure 4.2: Histograms of the generated domain thicknesses t_i for fixed parameters of the normal distribution ($t_\mu = 3\Lambda_L$, $t_\sigma = 0.5\Lambda_L$) and different total numbers of crystal domains $N_{\text{Layer}} \cdot N_{\text{Stat}}$. Solid line: ideal normal probability distribution.

4.2 Lattice structure factor

For the numerical simulation of the X-ray diffraction by a specific crystal it is necessary know the complex values of the structure factor by different reflexions and wavelengths of X-rays. For the $\mathrm{BaTiO_3}$ crystal they are calculated by substituting table values [15] of the atomic scattering factors in (2.6). However, we have to know the structure factors not only for tabular parameters, but for the arbitrary wavelength. The solution of this problem is based on the interpolation of the existing data from tables and is described in detail in the work of S.A.Stepanov and O.M.Lugovskaya [16].

Additionally, there is the method of a such modification of the structure factor, that it will be possible to take into account the influence of quadrupole transitions on the absorption in Borrmann spectroscopy [17]. The dynamical theory omits the quadrupole absorption, which can be sufficiently strong in X-ray absorption near edge structure (XANES), therefore M. Tolkiehn [18] has devised the artificial supplement to the structure factor, which imitates the quadrupole absorption, and specifically the electric dipole (E1) and electric quadrupole (E2) transitions in Ti, which are situated in the spectrum close to the 1s-3d transition. The theoretical principle of this modification is described in [19]. Also some experimental values for this model were borrowed from [20].

4.3 Propagation grid

Every wavefield splits into two separate wavefields after the propagation via every layer of the mosaic crystal: to one refracted and one reflected beam. Therefore, the number of the wavefields grows by every layer with power of two. To reduce the amount of required calculations we should introduce the following concept. Suppose the each domain is not thin; then the intensity of the reflected beam is significantly less than of the refracted beam. Therefore we will omit all beams inside the crystal, which are reflected more than one time (see Fig. 4.3). As a consequence, one beam comes out in the same direction as the incident beam after N_{Layer} refractions and N_{Layer} beams interferer in the direction of reflection after one reflection and $(N_{\text{Layer}} - 1)$ refractions. Results of such simulations are produced in the next part.

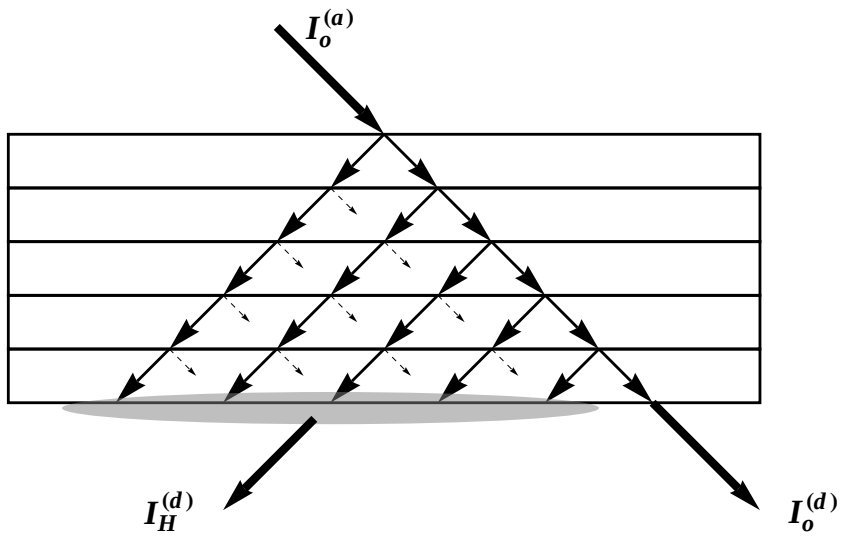

Figure 4.3: Beam propagation grid in the multilayer crystal. Beams, which are reflected more than one time, are omitted (dashed arrows). $I_0^{(a)}$: incident beam intensity; $I_0^{(d)}$: intensity of the N_{Layer} times refracted incident beam; $I_H^{(d)}$: total intensity of the outgoing beams in the direction of reflection.

4.4 Results

In this part will be shown numerical simulation results for X-ray diffraction by the $\mathrm{BaTiO_3}$ mosaic crystal on the (200) reflection. This choice was caused by pronounced Borrmann effect and relatively not strong absorption on this reflection. We suppose, the $\mathrm{BaTiO_3}$ lattice structure has a tetragonal form with lattice parameters $a = b = 3.986$ Å and $c = 4.026$ Å. The crystal model used in this simulation is comprised by 10 layers of domains with perfect lattice structure and with the mean thickness $t_\mu = 30\ \mu m$. The standard deviation of domain thickness is $t_\sigma = 2.5\ \mu m$. It means, that the total thickness of the mosaic crystal is $\approx 0.3\ mm$. Raw simulation results generated by the program are rocking curves of variations $I_0^{(d)}/I_0^{(a)}$ and $I_H^{(d)}/I_0^{(a)}$ with deviation from Bragg's angle $\Delta\theta$ of the incident wave for fixed energies and mosaicities. Typical rocking curves are shown in Fig. 4.4. The peaks of rocking curves are shifted relatively

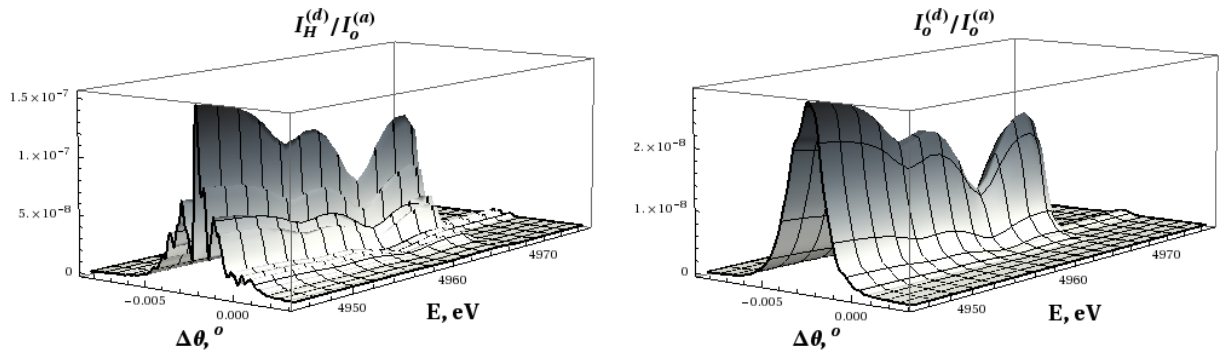

Figure 4.4: Variations $I_0^{(d)}/I_0^{(a)}$ and $I_H^{(d)}/I_0^{(a)}$ with deviation from Bragg's angle $\Delta\theta$ and energy for (200) reflection by the $\mathrm{BaTiO_3}$ mosaic crystal with parameters $t_\mu = 30\ \mu m$, $t_\sigma = 2.5\ \mu m$, $\omega_\sigma = 0.004°$, $N_{\mathrm{Layer}} = 10$, $N_{\mathrm{Stat}} = 300$.

to the point $\Delta\theta = 0$. This effect is caused by the absorption asymmetry for every diffracted beam (see Fig. 2.7, *left*). Dependencies of integrated rocking curves from energy and mosaicity are of interest for us and are shown below.

To make a comparison, in the beginning it was made the simulation of the diffraction process by a single-domain $0.3\ mm$ thick crystal. The variation of absorption with X-ray wave energy from 4945 eV to 4975 eV is shown in Fig. 4.5. This spectrum contains the electric dipole peak at 4960 eV (peak **D**) and electric quadrupole peak at 4953 eV (peak **Q**). The big peak at 4967 eV corresponds to the 1s-3d transition in Ti. However, simulations with the $0.3\ mm$

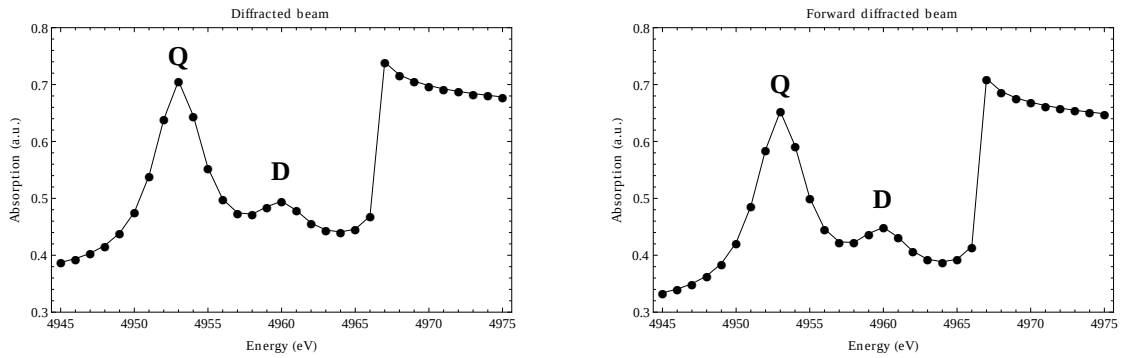

Figure 4.5: Simulated Ti *K* edge XANES spectra by (200) reflection of a $0.3\ mm$ thick perfect $\mathrm{BaTiO_3}$ crystal. **Q** and **D**: electric quadrupole and electric dipole peaks, respectively.

thick crystal composed of ten perfect crystals, which is physically the same as the previously simulated crystal, give us not the identical result (see Fig. 4.6). The reason is the fact that we omit a big part of diffracted wavefields inside the crystal, which is too rough for simulation

of the crystals with tiny imperfections. In this case the next order of approximation should be used (for example, by taking into account the beams shown as dashed in Fig. 4.3). Analogous

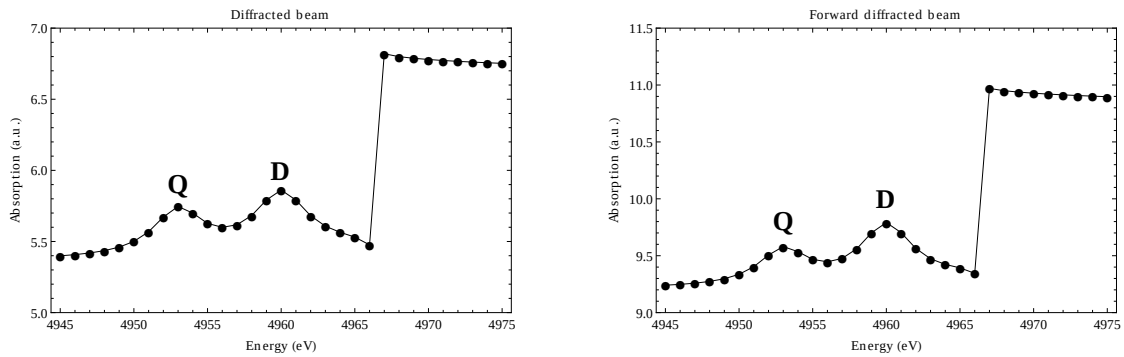

Figure 4.6: Simulated Ti *K* edge XANES spectra by (200) reflection of a $0.3\ mm$ thick $\mathrm{BaTiO_3}$ crystal composed of ten layers of perfect crystals. **Q** and **D**: electric quadrupole and electric dipole peaks, respectively.

energy spectrum for mosaic crystal shows (see Fig. 4.7) the increased absorption caused by defects of crystal structure. Positions of the absorption edge and quadrupole absorption peaks are evidently the same, but their proportions have been changed respectively to each other.

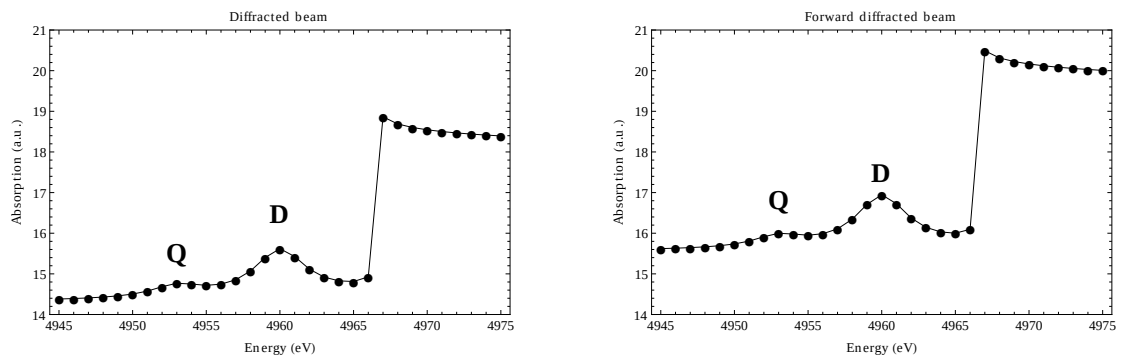

Figure 4.7: Simulated Ti *K* edge XANES spectra by (200) reflection of a $0.3\ mm$ thick mosaic $\mathrm{BaTiO_3}$ crystal with parameters $t_\mu = 30\ \mu m$, $t_\sigma = 2.5\ \mu m$, $\omega_\sigma = 0.004°$, $N_{\mathrm{Layer}} = 10$, $N_{\mathrm{Stat}} = 300$. **Q** and **D**: electric quadrupole and electric dipole peaks, respectively.

The influence of mosaicity to the Borrmann effect can be demonstrated by variations with mosaicity of integrated intensities by fixed wave energies before and after the absorption edge, which is shown in Fig. 4.8. Intensities of the beams in both reflected and forward diffracted directions are abating with growth of ω_σ. For large values of ω_σ the outgoing intensities are almost vanished. It means, that the Borrmann effect disappears with sufficient defects in the crystal.

Special interest is presented by variation of the ratio of quadrupole to dipole absorption coefficients with ω_σ (see Fig. 4.9). One can see, that the quadrupole absorption peak significantly grows in comparison with the dipole absorption peak with improvement of the crystal quality.

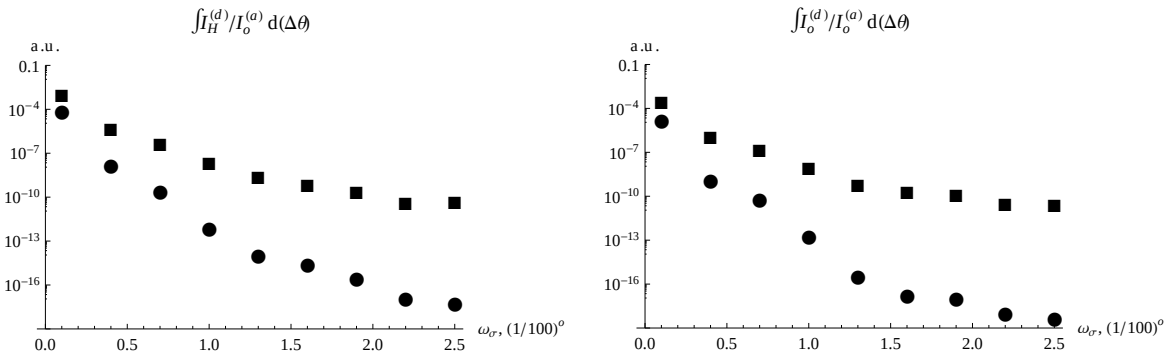

Figure 4.8: Variations the outgoing intensities with ω_σ for 4945 eV (*squares*) and 4968 eV (*circles*) by (200) reflection of a $0.3\ mm$ thick mosaic $\mathrm{BaTiO_3}$ crystal with parameters $t_\mu = 30\ \mu m$, $t_\sigma = 2.5\ \mu m$, $N_{\mathrm{Layer}} = 10$, $N_{\mathrm{Stat}} = 300$.

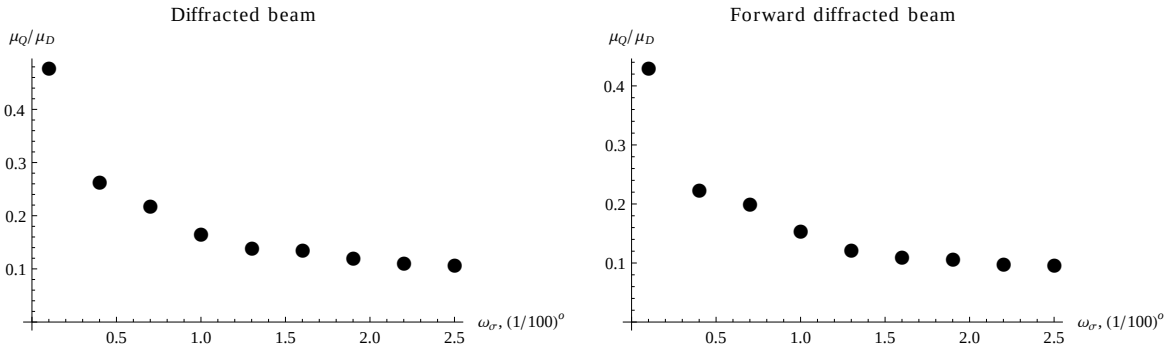

Figure 4.9: Variations of the ratio of absorption coefficients of quadrupole (at 4953 eV) and dipole (at 4960 eV) peaks with ω_σ by (200) reflection of a $0.3\ mm$ thick mosaic $\mathrm{BaTiO_3}$ crystal with parameters $t_\mu = 30\ \mu m$, $t_\sigma = 2.5\ \mu m$, $N_{\mathrm{Layer}} = 10$, $N_{\mathrm{Stat}} = 300$.

Chapter 5

Conclusion and Outlook

In this work the method of diffraction simulation for Borrmann spectroscopy in mosaic crystals was developed. Therefore, the theory, which described diffraction processes in a single perfect crystal, was applied to the complex system of many crystals. The method was implemented in code and tested for the model of the $\mathrm{BaTiO_3}$ multidomain crystal. The results of this simulations qualitative satisfy the initial expectations for medium orders of crystal defects, but are too rough for the crystals with tiny imperfections. In future the next orders of approximations should be used. Additionally, the models, used in simulations, needs to be specified to have future possibility of quantitative comparison with experiments. Also computing powers for simulations should be increased, for example, by computing on graphics processing units (GPUs), for a better simulation precision and reducing of computation time for more complicated crystal models.

Appendix A

Source code

This appendix contains the source code of the program for Wolfram Mathematica computation system, which was used for the numerical simulations made in this work.

```
<< Crystallography8`

(* ---Crystal configurations---*)
BTO = SetupCrystal[
   {{"Ba", 0, 0, 0}, {"Ti", .5, .5, .5},
    {"O", .5, .5, 0}, {"O", 0, .5, .5},
    {"O", .5, 0, .5}},
   Lattice → Tetragonal[3.992, 4.036]];
```

$$l[a_, x0_, x_] := \frac{1}{\pi} \frac{a}{a\,\hat{}\,2 + (x - x0)\,\hat{}\,2}$$

```
ll[x_] := l[.002, 4.953, x]
TiO2x =
  {Atoms → {{"Ti", 0, 0, 0, 1, 0},
     {"Ti", 0.5`, 0.5`, 0.5`, 1, 0},
     {"Ti", 0.25`, 0.25`, 0.25`, x, 0},
     {"Ti", 0.75`, 0.75`, 0.75`, x, 0},
     {"O", 0.301873`, 0.301873`, 0.`, 1, 0},
     {"O", 0.698127`, 0.698127`, 0.`, 1, 0},
     {"O", 0.801873`, 0.198127`, 0.5`, 1, 0},
     {"O", 0.198127`, 0.801873`, 0.5`, 1, 0}},
   CoordinateSystem →
    {{4.5845`, 0.`, 0.`}, {0.`, 4.5845`, 0.`},
     {0.`, 0.`, 2.9533`}},
   Metrik → {{0.04757908062490507`, 0.`, 0.`},
     {0.`, 0.04757908062490507`, 0.`},
     {0.`, 0.`, 0.11465285381977028`}},
   FData →
    {{1.2807` + 1.9021` e^(-116.105` #2^2) + 1.6991` e^(-35.6338` #2^2) +
        9.7595` e^(-7.8508` #2^2) + 7.3558` e^(-0.5` #2^2) +
        Cromer[22, 1000 #1] &, 0, 0, 0, 1, 0},
     {1.2807` + 1.9021` e^(-116.105` #2^2) + 1.6991` e^(-35.6338` #2^2) +
        9.7595` e^(-7.8508` #2^2) + 7.3558` e^(-0.5` #2^2) +
        Cromer[22, 1000 #1] &, 0.5`, 0.5`, 0.5`, 1, 0},
     {I ll[#1] &, 0.25`, 0.25`, 0.25`, x, 0},
```

```
      {I ll[#1] &, 0.75‘, 0.75‘, 0.75‘, x, 0},
      {I ll[#1 - .007] &, 0., 0., 0., 200 x, 0},
      {I ll[#1 - .007] &, 0.5, 0.5, 0.5, 200 x, 0},
      {0.2508‘ + 0.867‘ e^(-32.9089‘ #2^2) + 3.0485‘ e^(-13.2771‘ #2^2) +
         2.2868‘ e^(-5.7011‘ #2^2) + 1.5463‘ e^(-0.3239‘ #2^2) +
         Cromer[8, 1000 #1] &, 0.301873‘, 0.301873‘,
       0.‘, 1, 0},
      {0.2508‘ + 0.867‘ e^(-32.9089‘ #2^2) + 3.0485‘ e^(-13.2771‘ #2^2) +
         2.2868‘ e^(-5.7011‘ #2^2) + 1.5463‘ e^(-0.3239‘ #2^2) +
         Cromer[8, 1000 #1] &, 0.698127‘, 0.698127‘,
       0.‘, 1, 0},
      {0.2508‘ + 0.867‘ e^(-32.9089‘ #2^2) + 3.0485‘ e^(-13.2771‘ #2^2) +
         2.2868‘ e^(-5.7011‘ #2^2) + 1.5463‘ e^(-0.3239‘ #2^2) +
         Cromer[8, 1000 #1] &, 0.801873‘, 0.198127‘,
       0.5‘, 1, 0},
      {0.2508‘ + 0.867‘ e^(-32.9089‘ #2^2) + 3.0485‘ e^(-13.2771‘ #2^2) +
         2.2868‘ e^(-5.7011‘ #2^2) + 1.5463‘ e^(-0.3239‘ #2^2) +
         Cromer[8, 1000 #1] &, 0.198127‘, 0.801873‘,
       0.5‘, 1, 0}}};
BTOx =
  {Atoms → {{Ba, 0, 0, 0, 1, 0},
      {Ti, 0.5‘, 0.5‘, 0.515‘, 1, 0},
      {Ti, 0.75‘, 0.75‘, 0.765‘, x, 0},
      {O, 0.5‘, 0.5‘, 0.976‘, 1, 0},
      {O, 0, 0.5‘, 0.48‘, 1, 0}, {O, 0.5‘, 0, 0.48‘, 1, 0}},
   CoordinateSystem →
    {{3.986‘, 0.‘, 0.‘}, {0.‘, 3.986‘, 0.‘},
     {0.‘, 0.‘, 4.0262586‘}},
   Metrik → {{0.06293980764084228‘, 0.‘, 0.‘},
     {0.‘, 0.06293980764084228‘, 0.‘},
     {0.‘, 0.‘, 0.06168742884358552‘}},
   FData →
```

```
{{2.7731` + 2.6959` ⅇ^(-167.202` #2^2) + 10.888` ⅇ^(-20.2073` #2^2) +
    20.3361` ⅇ^(-3.216` #2^2) + 19.297` ⅇ^(-0.2756` #2^2) +
    Cromer[56, 1000 #1] &, 0, 0, 0, 1, 0},
 {1.2807` + 1.9021` ⅇ^(-116.105` #2^2) + 1.6991` ⅇ^(-35.6338` #2^2) +
    9.7595` ⅇ^(-7.8508` #2^2) + 7.3558` ⅇ^(-0.5` #2^2) +
    Cromer[22, 1000 #1] &, 0.5`, 0.5`, 0.515`, 1, 0},
 {I ll[#1] &, 0.75`, 0.75`, 0.765`, x, 0},
 {I ll[#1 - 0.007] &, 0.5`, 0.5`, 0.515`, 40 x, 0},
 {0.2508` + 0.867` ⅇ^(-32.9089` #2^2) + 3.0485` ⅇ^(-13.2771` #2^2) +
    2.2868` ⅇ^(-5.7011` #2^2) + 1.5463` ⅇ^(-0.3239` #2^2) +
    Cromer[8, 1000 #1] &, 0.5`, 0.5`, 0.976`, 1, 0},
 {0.2508` + 0.867` ⅇ^(-32.9089` #2^2) + 3.0485` ⅇ^(-13.2771` #2^2) +
    2.2868` ⅇ^(-5.7011` #2^2) + 1.5463` ⅇ^(-0.3239` #2^2) +
    Cromer[8, 1000 #1] &, 0, 0.5`, 0.48`, 1, 0},
 {0.2508` + 0.867` ⅇ^(-32.9089` #2^2) + 3.0485` ⅇ^(-13.2771` #2^2) +
    2.2868` ⅇ^(-5.7011` #2^2) + 1.5463` ⅇ^(-0.3239` #2^2) +
    Cromer[8, 1000 #1] &, 0.5`, 0, 0.48`, 1, 0}}};
TiO2q = TiO2x /. {x → 0.00002};
BTOq = BTOx /. {x → 0.00012};
```

```
InitDiffraction[ene_] := (
  hkl = {2, 0, 0};
  cry = BTOq;
  StrF = CalcFH[cry, ene, hkl];
  StrF0 = CalcFH[cry, ene, {0, 0, 0}];
  GAMMA = DGamma[ene, cry];
  chi0 = -GAMMA * CalcFH[cry, ene, {0, 0, 0}];
  mu0 = Mu0[cry, ene];
  k0 = 1 / Lambda[ene];
  nk = (1 + Re[chi0] / 2) k0;
  SinBr = Lambda[ene] *
    Norm[Inverse[BTO[[2, 2]]].hkl] / 2;
  CosBr = Sqrt[1 - SinBr^2];
 )

gammah[omega_] := Cos[omega] CosBr + Sin[omega] SinBr;
gamma0[omega_] := Cos[omega] CosBr - Sin[omega] SinBr;
AsRatio[omega_] := gamma0[omega] / gammah[omega];

DevPar[dth_, omega_] :=
 (dth * 2 * SinBr * CosBr * AsRatio[omega] -
    0.5 * chi0 * (1 - AsRatio[omega])) /
  (GAMMA * Sqrt[Abs[AsRatio[omega]]] * Sqrt[StrF * StrF])
```

```
xi0a[dth_, omega_] :=
 0.5 * k0 * Sqrt[Abs[AsRatio[omega]]] * GAMMA *
  Sqrt[StrF * StrF]
  (DevPar[dth, omega] +
    Sqrt[DevPar[dth, omega] ^ 2 + Sign[AsRatio[omega]]])
xi0b[dth_, omega_] :=
 0.5 * k0 * Sqrt[Abs[AsRatio[omega]]] * GAMMA *
  Sqrt[StrF * StrF]
  (DevPar[dth, omega] -
    Sqrt[DevPar[dth, omega] ^ 2 + Sign[AsRatio[omega]]])
xiha[dth_, omega_] :=
 0.5 * k0 * GAMMA *
  Sqrt[StrF * StrF] / Sqrt[Abs[AsRatio[omega]]] /
   (DevPar[dth, omega] +
     Sqrt[DevPar[dth, omega] ^ 2 + Sign[AsRatio[omega]]])
xihb[dth_, omega_] :=
 0.5 * k0 * GAMMA *
  Sqrt[StrF * StrF] / Sqrt[Abs[AsRatio[omega]]] /
   (DevPar[dth, omega] -
     Sqrt[DevPar[dth, omega] ^ 2 + Sign[AsRatio[omega]]])
mu0effa[dth_, omega_] := mu0 - 4 π * Im[xi0a[dth, omega]]
mu0effb[dth_, omega_] := mu0 - 4 π * Im[xi0b[dth, omega]]
```

```
E0a[dth_, omega_, t_] :=
 Exp[-mu0effa[dth, omega] * t / gamma0[omega]] *
  ( Sqrt[1 + Re[DevPar[dth, omega]]^2]  -
      DevPar[dth, omega] )^2  /
   ( 4 (1 + Re[DevPar[dth, omega]]^2))
E0b[dth_, omega_, t_] :=
 Exp[-mu0effb[dth, omega] * t / gamma0[omega]] *
  ( Sqrt[1 + Re[DevPar[dth, omega]]^2]  +
      DevPar[dth, omega] )^2  /
   ( 4 (1 + Re[DevPar[dth, omega]]^2))
EHa[dth_, omega_, t_] :=
 Exp[-mu0effa[dth, omega] * t / gamma0[omega]] *
  AsRatio[omega] / ( 4 (1 + Re[DevPar[dth, omega]]^2))
EHb[dth_, omega_, t_] :=
 Exp[-mu0effb[dth, omega] * t / gamma0[omega]] *
  AsRatio[omega] / ( 4 (1 + Re[DevPar[dth, omega]]^2))
```

```
PLambda[omega_] :=
 Sqrt[Abs[gammah[omega]] * gamma0[omega]] / k0 / GAMMA /
  Re[Sqrt[StrF * StrF]]
PP[dth_, omega_] :=
 Sqrt[1 + Re[DevPar[dth, omega]] ^ 2] / PLambda[omega]
I0na[dth_, omega_, t_] :=
 1 / ( 4 (1 + Re[DevPar[dth, omega]] ^ 2)) *
  ((1 + Re[DevPar[dth, omega]] ^ 2) (1 + 1) +
    2 Cos[2 π * t * PP[dth, omega]])
IHna[dth_, omega_, t_] :=
 1 / ( 4 (1 + Re[DevPar[dth, omega]] ^ 2)) *
  ((1 + 1) - 2 Cos[2 π * t * PP[dth, omega]])
IH[dth_, omega_, t_] :=
 1 / ( 4 (1 + Re[DevPar[dth, omega] ^ 2])) * (
   (Exp[- mu0effa[dth, omega] * t / gamma0[omega]] +
      Exp[- mu0effb[dth, omega] * t / gamma0[omega]])
    - 2 Cos[2 π * t * PP[dth, omega]] *
     (Exp[- (mu0effa[dth, omega] + mu0effb[dth, omega]) *
        t / gamma0[omega] / 2]))
I0[dth_, omega_, t_] :=
 1 / ( 4 (1 + Re[DevPar[dth, omega]] ^ 2)) * (
   (1 + 2 * Re[DevPar[dth, omega]] ^ 2 -
       2 * Re[DevPar[dth, omega]] *
        Sqrt[1 + Re[DevPar[dth, omega]] ^ 2]) *
     Exp[- mu0effa[dth, omega] * t / gamma0[omega]]
    +
    (1 + 2 * Re[DevPar[dth, omega]] ^ 2 +
       2 * Re[DevPar[dth, omega]] *
        Sqrt[1 + Re[DevPar[dth, omega]] ^ 2]) *
     Exp[- mu0effb[dth, omega] * t / gamma0[omega]]
    + 2 Cos[2 π * t * PP[dth, omega]] *
     (Exp[- (mu0effa[dth, omega] + mu0effb[dth, omega]) *
        t / gamma0[omega] / 2]))
```

```
D0[dth_, omega_, t_] :=
 1/2*
   (-DevPar[dth, omega]/Sqrt[1+DevPar[dth, omega]^2]+
     1)*
   Exp[-2*π*ⅈ*t*(xi0a[dth, omega]+k0*chi0/2)/
      gamma0[omega]]+
  1/2*
   (DevPar[dth, omega]/Sqrt[1+DevPar[dth, omega]^2]+
     1)*
   Exp[-2*π*ⅈ*t*(xi0b[dth, omega]+k0*chi0/2)/
      gamma0[omega]]
DH[dth_, omega_, t_] :=
 1/2*1/Sqrt[1+DevPar[dth, omega]^2]*
   Exp[-2*π*ⅈ*t*(xi0a[dth, omega]+k0*chi0/2)/
      gamma0[omega]]-
  1/2*1/Sqrt[1+DevPar[dth, omega]^2]*
   Exp[-2*π*ⅈ*t*(xi0b[dth, omega]+k0*chi0/2)/
      gamma0[omega]]

GenerateCrystal[NLayers_, Omega_, SigmaOmega_,
  t_, Sigmat_] :=
 {
  (*All structure parameters*)
  RandomVariate[NormalDistribution[Omega, SigmaOmega],
   NLayers], (*Lattice asymmetry*)
  RandomVariate[NormalDistribution[t, Sigmat], NLayers]
  (*Crystals' thickness*)
 }

FullI[DTheta_, Layers_] := Module[{NLayers, i, j, m},
  (
   NLayers = Length[Layers[[1]]];
   Beams = {
     Table[1, {NLayers+1}],
     (*Relative complex amplitudes of beams*)
     Table[DTheta, {NLayers+1}]};
   (*Delta theta for each beam*)
   (*Here we go*)
```

```
    For[i = 1, i <= NLayers, i ++,
     For [j = 1,  j ≤ i - 1,  j ++,
      Beams[[2, j]] = Beams[[2, j]] - Layers[[1, i]];
      Beams[[1, j]] = Beams[[1, j]] *
        D0[Beams[[2, j]], -Layers[[1, i]],
         Layers[[2, i]]];
      Beams[[2, j]] = Beams[[2, j]] /
        AsRatio[-Layers[[1, i]]];
     ];

     Beams[[2, i]] = Beams[[2, i]] + Layers[[1, i]];
     Beams[[1, i]] = Beams[[1, NLayers + 1]] *
       DH[Beams[[2, i]], Layers[[1, i]], Layers[[2, i]]];
     Beams[[2, i]] =
      Beams[[2, i]] / AsRatio[Layers[[1, i]]];

     Beams[[2, NLayers + 1]] =
      Beams[[2, NLayers + 1]] + Layers[[1, i]];
     Beams[[1, NLayers + 1]] =
      Beams[[1, NLayers + 1]] *
       D0[Beams[[2, i]], Layers[[1, i]], Layers[[2, i]]];
     Beams[[2, NLayers + 1]] =
      Beams[[2, NLayers + 1]] / AsRatio[Layers[[1, i]]];
    ];
    (*Sending results back*)
    Return[{
      Abs[Sum[Beams[[1, m]], {m, 1, NLayers}]] ^ 2,
      (*Reflected beams*)
      Abs[Beams[[1, NLayers + 1]]] ^ 2 (*Refracted beam*)
     }];
   )]

(* -------------------------*)
ResetDirectory[];
SetDirectory["bachelor/mathematica/simdata/15"];
(* ---Header file and simulation parameters---*)
"Simulation of Laue X-ray diffraction in a
   multilayer crystal" >> HEADER.txt
```

```
"Aram Kalaydzhyan" >>> HEADER.txt
$MachineName >>> HEADER.txt
DateString[] >>> HEADER.txt
" " >>> HEADER.txt
"Crystal:" >>> HEADER.txt
"BTO with quadrupole absorption" >>> HEADER.txt
"Energy, kEv:" >>> HEADER.txt
En = Table[e, {e, 4.93, 4.97, 0.001}] >>> HEADER.txt
"Reflection:" >>> HEADER.txt
hkl >>> HEADER.txt
"Number of layers in the crystal:" >>> HEADER.txt
NLayers = 20 >>> HEADER.txt
"Normal thickness of every layer, A:" >>> HEADER.txt
LTm = 200 000 >>> HEADER.txt
"Thickness dispersion, A:" >>> HEADER.txt
LTs = 50 000 >>> HEADER.txt
"Normal assymetry of the crystal lattice, grad:" >>>
 HEADER.txt
LOmega = 0 >>> HEADER.txt
"Assymetry dispersions, 1/100 grad:" >>> HEADER.txt
Def = {0.5} >>> HEADER.txt
"Number of MC-simulations:" >>> HEADER.txt
MCStat = 50 >>> HEADER.txt
(* -------------------------*)

IntSpectrum = Table[{0, 0, 0}, {Length[En]}];
For[ne = 1, ne ≤ Length[En], ne ++,
  InitDiffraction[En[[ne]]];
  For[nd = 1, nd ≤ Length[Def], nd ++,
   MCSpectrum = 0;
   For[st = 1, st ≤ MCStat, st ++,
    Crystal = GenerateCrystal[NLayers, LOmega,
      Def[[nd]] / 100 * π / 180, LTm, LTs];
    Spectrum = ParallelTable[{x, FullI[x, Crystal][[k]]},
      {k, 2}, {x, -0.0003, 0.0001, 0.000002}];
    MCSpectrum = MCSpectrum + Spectrum;
   ];
   MCSpectrum = MCSpectrum / MCStat;
```

```
    Export[
     StringJoin[{"MCSp_", ToString[En[[ne]]], ".txt"}],
     {MCSpectrum[[1]]ᵀ[[1]], MCSpectrum[[1]]ᵀ[[2]],
        MCSpectrum[[1]]ᵀ[[2]]}ᵀ // TableForm, "CSV"];
    Export[StringJoin[{"MCSp_R_", ToString[En[[ne]]],
       ".pdf"}], ListPlot[MCSpectrum[[1]],
      PlotRange → All]];
    Export[StringJoin[{"MCSp_T_", ToString[En[[ne]]],
       ".pdf"}], ListPlot[MCSpectrum[[2]],
      PlotRange → All]];
    IntSpectrum[[ne]] =
     {En[[ne]], Total[MCSpectrum[[1]]ᵀ[[2]]],
      Total[MCSpectrum[[2]]ᵀ[[2]]]};
   ];
  ];
Export[StringJoin[{"IntSpectrum.txt"}],
  IntSpectrum // TableForm, "CSV"];
Export[StringJoin[{"IntSpectrum_R.pdf"}],
  ListPlot[{IntSpectrumᵀ[[1]], IntSpectrumᵀ[[2]]}ᵀ,
   PlotRange → All]];
Export[StringJoin[{"IntSpectrum_T.pdf"}],
  ListPlot[{IntSpectrumᵀ[[1]], IntSpectrumᵀ[[3]]}ᵀ,
   PlotRange → All]];
(* -------------------------*)
" " >>> HEADER.txt
DateString[] >>> HEADER.txt
(* -------------------------*)
```

Bibliography

[1] C. G. Darwin, Phil. Mag. **27**, 315 (1914).

[2] P. P. Ewald, Ann. Phys. Lpz. **54**, 519 (1917).

[3] M. von Laue, Ergebnisse d. Exakt. Naturwissenschaften **10**, 207-284 (1931).

[4] A. Authier, *Dynamical Theory of X-Ray Diffraction*, (IUCr, 2003).

[5] Z. G. Pinsker, *Dynamical Scattering of X-Rays in Crystals*, (Springer-Verlag, 1978).

[6] W. H. Zachariasen, *Theory of X-rays Diffraction in Crystals* (Wiley, 1945).

[7] B. W. Batterman and H. Cole, Rev. Mod. Phys **36**, 681 (1964).

[8] G. Borrmann, Z. Physik **42**, 157 (1941).

[9] G. Borrmann, Z. Physik **127**, 297 (1950).

[10] P. P. Ewald, *Handbuch der Physik* **24**, 280 (Springer-Verlag, 1933).

[11] A. von Hippel, Rev. Mod. Phys **22**, 221 (1950).

[12] P. W. Forsbergh, Phys. Rev. **76**, 1187 (1949).

[13] H. F. Kay, Acta Cryst. **1**, 229 (1948).

[14] R. G. Rhodes, Acta Cryst. **4**, 105 (1951).

[15] *International Tables for X-ray Crystallography, vol.C* (Kluwer Acad. Publ., 1992).

[16] O. M. Lugovskaya and S. A. Stepanov, Sov. Phys. Crystallogr. **36**, 478 (1991).

[17] R. F. Pettifer, S. P. Collins, D. Laundy, Nature **454**, 196 (2008).

[18] Personal communication with Dr. M. Tolkiehn.

[19] M. Tolkiehn, T. Laurus, S. P. Collins, Phys. Rev. B **84**, 241101 (2011).

[20] A. I. Frenkel *et al.*, Phys. Rev. Lett. **99**, 215502 (2007).